RSC Sustainability

ROYAL SOCIETY OF CHEMISTRY

PAPER

View Article Online
View Journal | View Issue

Cite this: *RSC Sustainability*, 2025, **3**, 4794

Polyaniline-functionalized biochar (PANI@ALB) as a heterogeneous acid–base bifunctional catalyst for one-pot cascade reactions under green reaction conditions

Nida Khan,[a] Mohd Umar Khan,[a] Mo Shadab,[b] M. B. Siddiqui[b] and Zeba N. Siddiqui *[a]

Received 15th April 2025
Accepted 1st August 2025

DOI: 10.1039/d5su00279f

rsc.li/rscsus

A sustainable, eco-friendly, and economical approach is developed to design a well-architectured polyaniline-functionalized biochar (PANI@ALB) as an acid–base bifunctional heterocatalyst for one-pot cascade reactions involving the synthesis of complex 2-amino-4*H*-pyran-3-carbonitrile derivatives. The activated biochar (ALB), derived from the pyrolysis of lac tree (*Schleichera oleosa*) leaves, is intercalated with PANI nanosheets *via* an *in situ* acid-catalyzed oxidative polymerization process to obtain PANI@ALB, the desired acid–base catalytic system. PANI@ALB exhibits enhanced catalytic activity compared to biochar or polyaniline (PANI). The superior performance of PANI@ALB has been ascribed to the synergistic effect between H^+ and –NH– & = N– of biochar and PANI, respectively, confirmed by the Hammett indicator method. The synthesized catalyst exemplified remarkably high atom economy (95%), excellent recyclability (87% after the 10th cycle), and exceedingly high turnover frequency (TOF), which collectively vouched for this protocol to be reckoned as a greener and more sustainable alternative compared to previously existing methodologies, thereby sharing the podium with some of the best catalysts known for such results.

Sustainability spotlight

A sustainable approach for the synthesis of 2-amino-4*H*-pyran-3-carbonitrile derivatives has been developed involving *Schleichera oleosa* leaf-derived biochar incorporated with polyaniline as a recyclable catalyst. The simple reaction procedure, ambient temperature, recyclability for up to ten cycles, high atom economy, and low E-factor suggest the greenness of the proposed method. The as-synthesized catalyst is non-toxic and has a high surface area due to large pores present on the surface of the catalyst, enabling the decrement of activation energy. The high recyclability of the catalyst also shows that no leaching of the catalyst occurred during the course of the reaction.

1 Introduction

Acid–base bifunctional catalysts possess both acidic and basic active sites, facilitating reactions requiring simultaneous acid and base catalysis. There has been a lot of interest in chemical processes cooperatively facilitated by solid acid–base bifunctional catalysts having excellent catalytic activities and active site dispersion.[1–3] The dual functionality of acid–base systems allows for cooperative activation of reactants, enhancing reaction efficiency and selectivity in various organic transformations involving cascade processes.[4] Homogeneous catalysis prevents one-pot cascade processes due to acid–base neutralization. However, they could be accomplished using heterogeneous catalytic systems because the restricted movement of acidic and basic groups does not allow them to be in direct contact. Developing such catalysts has been a focal point in designing environmentally friendly and efficient catalytic processes. A notable example is the synthesis of perovskite-type oxides, which have been tailored to exhibit both acidic and basic properties, which in turn show remarkable catalytic performance in reactions like the cyanosilylation of carbonyl compounds, showcasing their potential in acid–base catalysis.[4]

Biochar, a carbon-rich material produced through the pyrolysis (high-temperature decomposition in the absence of oxygen) of organic biomass, is gaining tremendous attention as an effective material for catalyst support in various chemical reactions because it can be employed both as an eco-friendly and economically viable alternative, presenting itself as a viable alternative source to conventional catalysts.[5,6] It is typically associated with a highly porous structure, which increases the surface area and active sites available for catalytic reactions. The

[a]*Green Chemistry Laboratory, Organic Chemistry Division, Department of Chemistry, Aligarh Muslim University, Aligarh, 202002, India. E-mail: nidakhan71321@gmail.com; umar.chem786@gmail.com; siddiqui_zeba@yahoo.co.in*

[b]*Allelopathy and Plant Taxonomy Laboratory, Department of Botany, Aligarh Muslim University, Aligarh, UP, India, 202002. E-mail: shadabalig89@gmail.com; zaman.amu@gmail.com*

surface of biochar-based functional materials possesses abundant functional moieties, namely hydroxyl, carboxyl, and carbonyl groups, thereby facilitating the adsorption of reactants or providing active sites for catalytic processes[7,8]

Despite all of these remarkable characteristics, biochar has been known to have drawbacks, such as poor mechanical stability and low catalytic activity, much like any other substance. Henceforth, activation followed by fabrication of the biochar with other polymer matrices, like polyaniline (PANI), polypyrrole, *etc.*, overcomes these barriers, improving the catalyst's overall efficiency.[9,10] These catalysts often exhibit tremendous surface areas, enabling the adsorption of reactants and facilitating reactions *via* substrate polarization or intermediate stabilization, typically through Lewis or Brønsted acid–base catalysis.[11–28] PANI, a phenyl-based polymer, was chosen on account of its chemically flexible imine (=N–) groups flanked by phenylene rings, which allow protonation, deprotonation, and other physicochemical interactions.[29] It is associated with other fascinating properties such as good electrical conductivity, multi-redox reaction ability, low cost, and ease of synthesis, which makes it a suitable material in catalyzing organic reactions.[30] Leveraging the complementary properties of polymers and biochar, several polymer-functionalized biochar catalysts have been employed to synthesize various heterocyclic compounds, including chromenes, pyranopyrazoles, pyrazolopyridines, tetrazoles, oxindole dihydropyridines, benzylpyrazolyl coumarins, quinazolinones, spirochromenes, and cyclic carbonates.[11–28]

Among the well-known heterocyclic compounds, poly substituted 2-amino-4*H*-pyran-3-carbonitrile derivatives are another class of essential heterocyclic compounds with a wide range of noteworthy biological activities namely antibacterial, anti-inflammatory, anti-tuberculosis, antimalarial, inducer of apoptosis, anticancer, inhibitor of the excitatory amino acid transporters (EAATs), *etc.*[31–35] Henceforth, the idea of a novel modified polycyclic framework based on this core structure has sparked a great deal of effort and attention, and their enormous potential in drug discovery has motivated a vast range of synthetic work.

Inspired by the applicability of functionalized biochar and biological activities of 2-amino-4*H*-pyran-3-carbonitrile derivatives, it is proposed herein to incorporate a polymer with catalytic functionalities onto activated biochar to enhance its catalytic efficacy. In this work, activated lac tree leaf biochar (ALB), derived from the leaves of *Schleichera oleosa*, was functionalized with PANI nanosheets *via in situ* acid-catalyzed oxidative polymerization of aniline. The resulting PANI@ALB decorated with both acidic and basic sites exhibited remarkable stability in air, at high temperatures, and under aqueous conditions, affirming it as optimal for organic processes under normal reaction conditions. This study introduces PANI@ALB as a recyclable, green, and heterogeneous catalyst for efficiently synthesizing complex fused heterocycles under sustainable conditions. No reports exist on applying a PANI-functionalized biochar composite (PANI@ALB) for organic synthesis. High yields, a good E-factor (range of 0.02–0.25), high atom economy (around 95%), high turnover numbers, and eco-compatibility highlight this protocol for providing new insights into green and sustainable synthesis of fused heterocycles *via* a biochar based functional material towards a sustainable platform carbon material and broaden the horizons of practical applications of PANI@ALB for synthesis of pharmacologically active heterocycles under ecologically sound conditions.

2 Materials and methods

The synthesis of the PANI@ALB catalyst is carried out in two steps. The first step involves the activation of biochar derived from the biomass feedstock of the lac tree (*Schleichera oleosa*) leaves. In the second step, ALB is added to an aniline solution, which is followed by an *in situ* polymerization process (Scheme 1).

2.1. Leaf characteristics

Leaves are paripinnate, with 2–4 pairs of pinnae. Leaflets are elliptical to elliptic-oblong, coriaceous, 4.5–18.5(−25) × 2.5–9 cm, dark brown or greyish-green above, lighter-brown to greenish beneath, deep purple when young, and have veins in 12–15 pairs, looped and joined near the margin. The leaf texture of *Schleichera oleosa* (Lour.) Oken is coriaceous. Wang *et al.* (2010) reported that coriaceous leaves contain a higher concentration of lignin and cellulose materials[36,37]

2.2. Synthesis of ALB

Activating biochar is essential for enhancing catalytic efficiency.[38] Herein, carbonized biochar is produced through pyrolysis of lac tree leaf biomass at 500 °C in a tube furnace in a nitrogen atmosphere for 4 hours. The heating rate was set at 10 °C min^{-1}. The lac tree biochar was left to cool naturally in the tube furnace. The biochar material was sieved using a 200 mesh screen as part of the process. In order to increase the surface area and porosity, the biochar was activated using KOH pellets (1 : 1 ratio of biochar to KOH pellets).[5] The mixture was stirred overnight to ensure a thorough dispersion of KOH in the biochar. After that, ultrasonication is employed to afford the smallest particles possible. The chemical activation increased the hydroxyl groups on the surface of ALB. The final products were filtered with a vacuum pump and were carefully rinsed multiple times with nano-pure water to ensure a pH-neutral condition. Later, ALB was dried at 80 °C in a vacuum oven for 24 hours and used for subsequent synthesis.

2.3. Synthesis of the PANI@ALB hybrid composite

The method of preparation for the PANI@ALB hybrid catalyst is as follows: concisely, the aniline monomer (2 mL) was transferred into a beaker containing 98 mL of a 0.1 M hydrochloric acid (HCl) solution, and stirring was continued for a few hours. To achieve a homogeneous mixture, the predetermined reactive ingredients were subjected to sonication for 25 min in an ultrasonic bath. The reaction components were further agitated with the aniline monomer for 1 hour. The ammonium per sulphate (APS) solution [0.274 M in 100 mL HCl (0.1 M)] was added dropwise into the above suspension inside an ice bath for

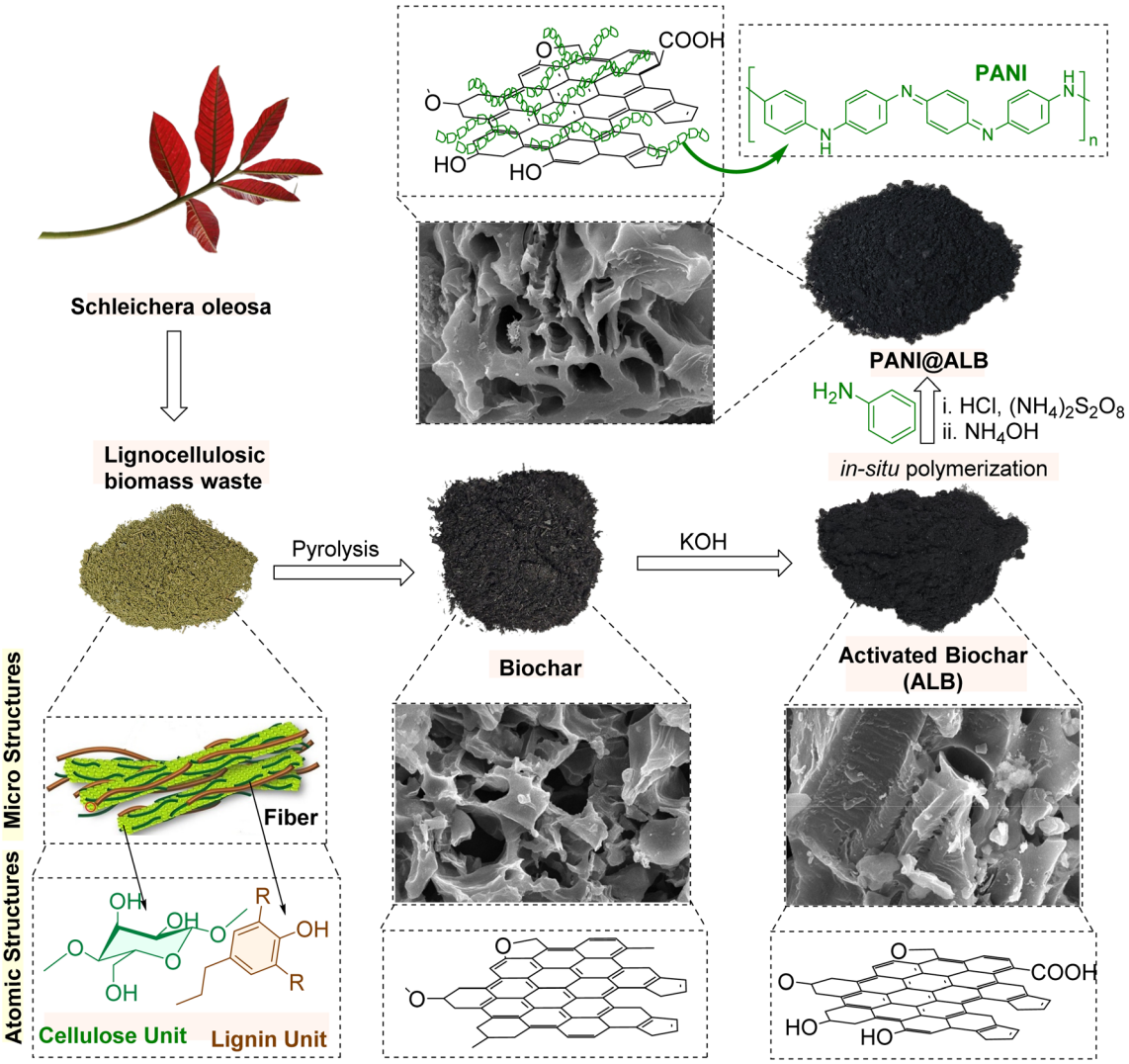

Scheme 1 Schematic representation for the synthesis of the acid–base bifunctional PANI@ALB catalyst.

30 minutes to commence the polymerization process. Thereafter, the suspension was stirred at room temperature for 12 h. Subsequently, the final product was isolated, rinsed with nano-pure water, and dried at 60 °C for 24 hours in a vacuum oven. The formed product was deprotonated by treatment with aqueous ammonia (3 wt%). The deprotonated composite was further washed with methanol and nano-pure water. The formed powder was denoted as a PANI@ALB hybrid catalyst.

3 Results and discussion

3.1. Characterization of the catalyst

3.1.1. FTIR analysis. The FTIR spectra were employed to analyse the bond characteristics and interaction nature of the PANI, ALB, and PANI@ALB catalysts. The FTIR spectra of PANI (Fig. 1) revealed an N–H stretching band at around 3252 cm^{-1} and a = C–H stretching band at 3033 cm^{-1}. The absorption bands at 1586 cm^{-1} show the quinonoid skeleton in the PANI, whereas the stretching vibrations of the benzenoid moiety appeared at 1496 cm^{-1}. The deformational and stretching bands of the C–N bond were at 1382 cm^{-1} and 1307 cm^{-1}, respectively. The vibrational bands at 1162 cm^{-1} and 824 cm^{-1} were attributed to plane and out-of-plane deformations of the C–H bond of 1,4-aromatic rings.[39] The FTIR spectrum of ALB (Fig. 1) showed stretching vibrations of –OH and aliphatic –CH at 3389 and around 2926 cm^{-1}, respectively. The symmetric stretching vibration of COO^- (1567 cm^{-1}), overlapping of aromatic CO– and phenolic –OH stretching of carboxylic acid (1377 cm^{-1}), and aromatic –CH stretching (756 cm^{-1})[40] further reaffirmed the structure of ALB. The IR spectrum of PANI@ALB revealed overlapped adsorption bands of pristine PANI and biochar. The absorption band at 1581 cm^{-1} corresponded to the stretching vibration of the quinonoid ring of PANI and the stretching vibration of COO^- of ALB. Compared to biochar, the FTIR spectrum of PANI@ALB revealed an increase in the peak intensity at 2930 cm^{-1}, which the incorporation of PANI might cause, enhancing the number of =C–H groups in the final catalyst. The peak heights of other functional groups and

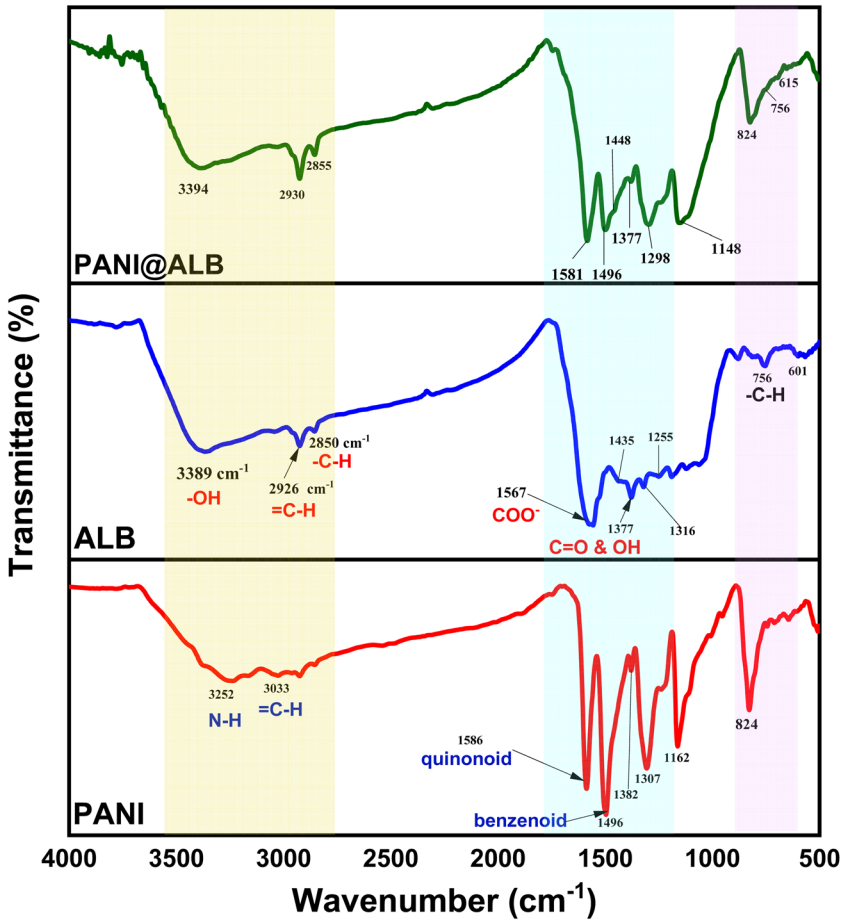

Fig. 1 FT-IR analysis of PANI, ALB, and PANI@ALB.

corresponding stretching frequencies of both biochar and PANI in the FTIR spectrum of PANI@ALB indicated the successful synthesis of the acid–base heterogeneous catalyst.

3.1.2. XRD analysis. Powder XRD analysis was employed to examine the crystalline and phase components of the catalysts. Fig. 2 shows the PXRD spectra of ALB, PANI, and the PANI@ALB

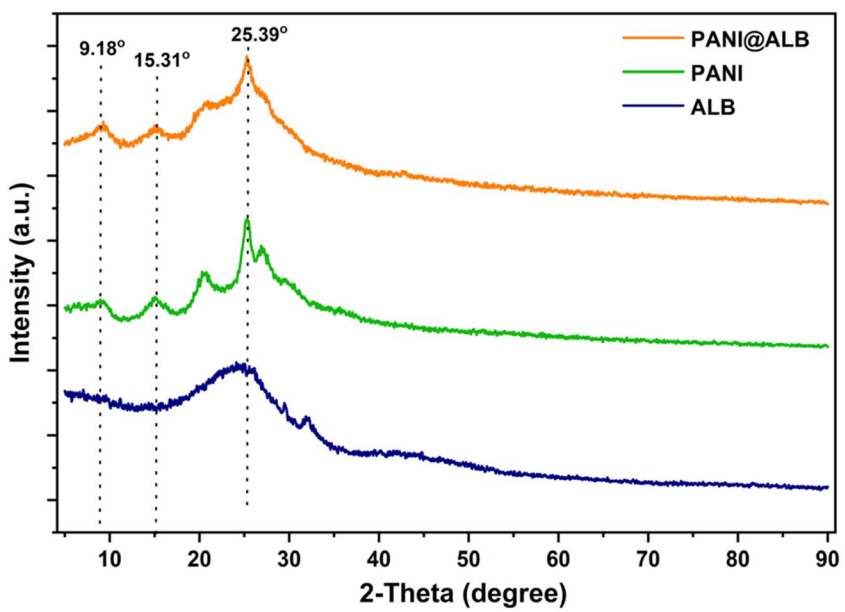

Fig. 2 XRD pattern of ALB, PANI, and the PANI@ALB catalyst.

catalyst. The XRD pattern of biochar generated after pyrolysis at a temperature of 500 °C affirmed the presence of cellulose planes as identified by using the peak located at 25°.[41,42] PANI showed characteristic peaks at 9.41° 15.04°, 20.50°, and 25.23°. The benzenoid and quinonoid rings were shown to repeat periodically by the two broad peaks of PANI at $2\theta = 20.50°$ (020 plane) and 25.23° (200 plane), respectively, which confirmed the semi-crystalline nature of PANI.[43,44] The PXRD spectra of the PANI@ALB material showed the distinctive peaks of PANI and biochar components. The peaks corresponding to biochar showed a unique change with respect to the peak heights, suggesting successful intercalation with PANI.

In addition, the Scherer equation (eqn (1)) was employed to calculate the sample crystallite size:

$$D = \frac{k\lambda}{\beta \cos \theta} \quad (1)$$

θ is the reflection angle, β is the reflection's full width and half maximum (FWHM), and k is the reflection constant. For ALB, PANI, and PANI@ALB, the crystallite size was determined to be 1.08, 2.21, and 2.00 nm, respectively, using eqn (1).

3.1.3. SEM-EDX analysis. SEM analysis provided an in-depth insight into the surface morphology and distribution of the prepared catalysts, as depicted in Fig. 3. The biochar surface

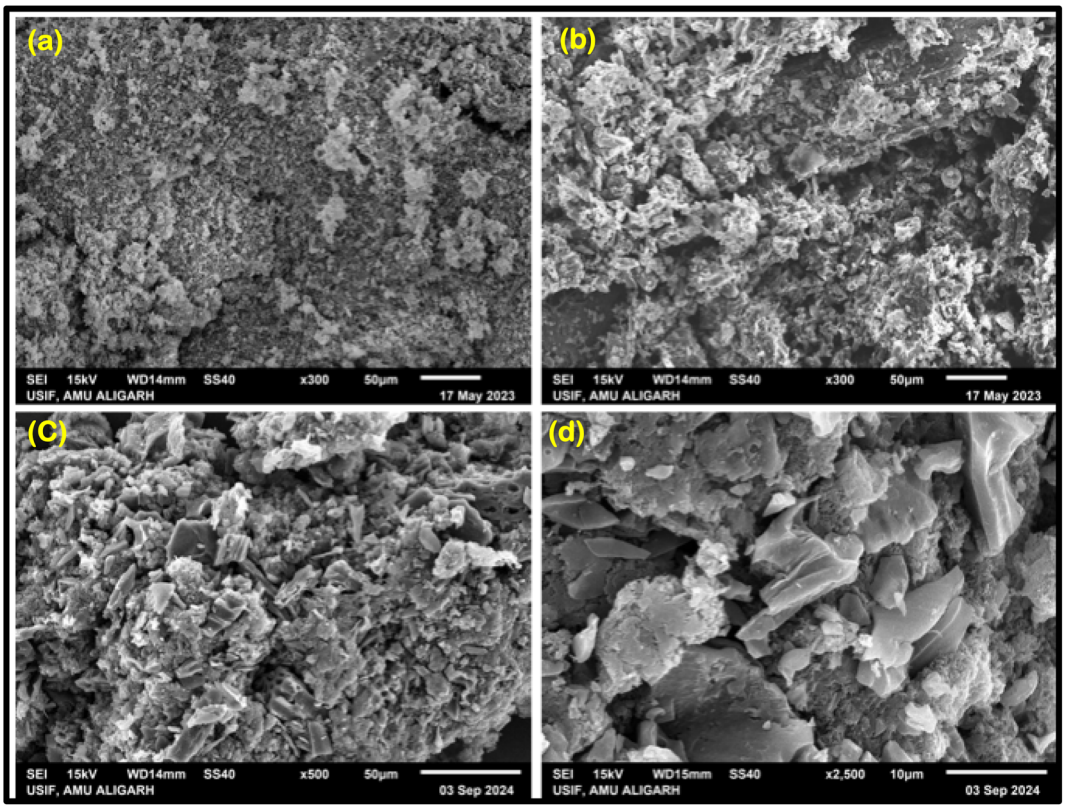

Fig. 3 SEM analysis of ALB (a and b) and PANI@ALB (c and d).

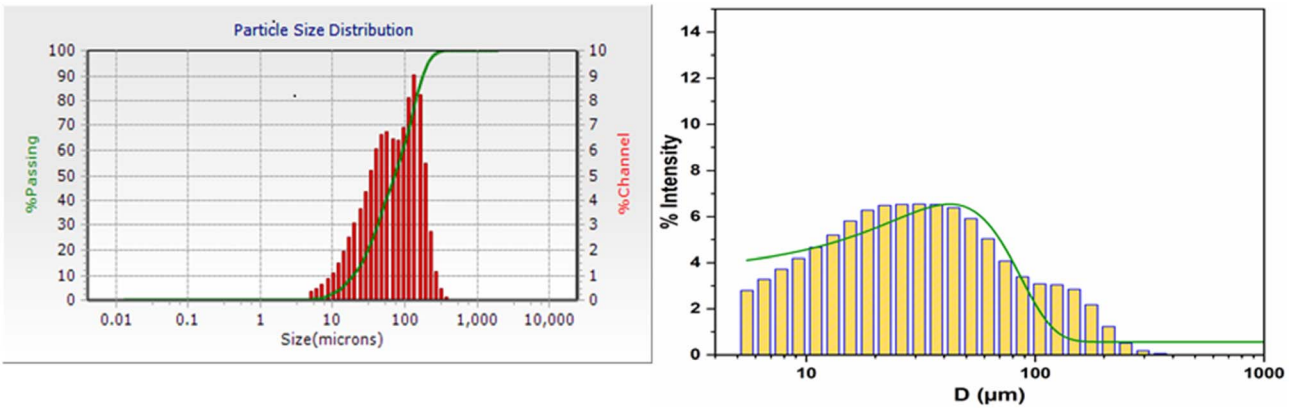

Fig. 4 Particle size distribution of PANI@ALB.

[Fig. 3(a) and (b)] revealed an open porous structure with an undefined pore size. Fig. 3(c) and (d) depict the surface morphology of PANI@ALB, which exhibited significant variations in the morphology of the biochar's structure on account of *in situ* polymerization with PANI, which resulted in the formation of the final catalyst. A PANI aggregate that camouflaged the biochar surface was also observed, suggesting successful catalyst synthesis.[39,45] Furthermore, it is inferred from the particle size distribution analysis (Fig. 4) that the particles were uniformly distributed. Based on the functionalization of biochar with PANI, relatively larger-sized particles (average size around 100 μm) were obtained. The results indicated that biochar and PANI were almost evenly distributed in the final catalyst, and networks in the polymer matrix were formed arbitrarily.

EDX analysis provided further evidence of the successful synthesis of the PANI@ALB catalyst. The EDX analysis of ALB [Fig. 5(a)] showed only the presence of carbon and oxygen elements, a characteristic feature of biochar. In contrast, the EDX analysis of PANI@ALB showed the presence of nitrogen in addition to carbon and oxygen, suggesting the successful embedment of PANI into biochar. Furthermore, the high percentage of nitrogen content in PANI@ALB compared to ALB correlated with the proportion of PANI in the composite, further supports the notion of the PANI@ALB composite's successful synthesis. The elemental mapping technique further revealed the uniform distribution of corresponding elements of ALB (Fig. 6) and PANI@ALB (Fig. 7), respectively. These revelations again indicated successful synthesis and uniform composition of the proposed catalyst.

3.1.4. Thermal analysis. The thermal stability of the catalysts was evaluated in the 25–800 °C range. Two distinct weight losses are observed at 100 °C and 412 °C for all the synthesized catalysts, respectively (Fig. 8). The first weight loss, at 100 °C, corresponded to the loss of adsorbed water molecules from the catalyst surface. ALB's subsequent significant weight loss from ~450 to 550 °C was attributed to thermal decompositions, including decarboxylation, decarbonylation, and carbon skeleton alterations.[46] PANI exhibited weight loss at lower temperatures, but for a more extensive range from ~350 to 630 °C.[47]

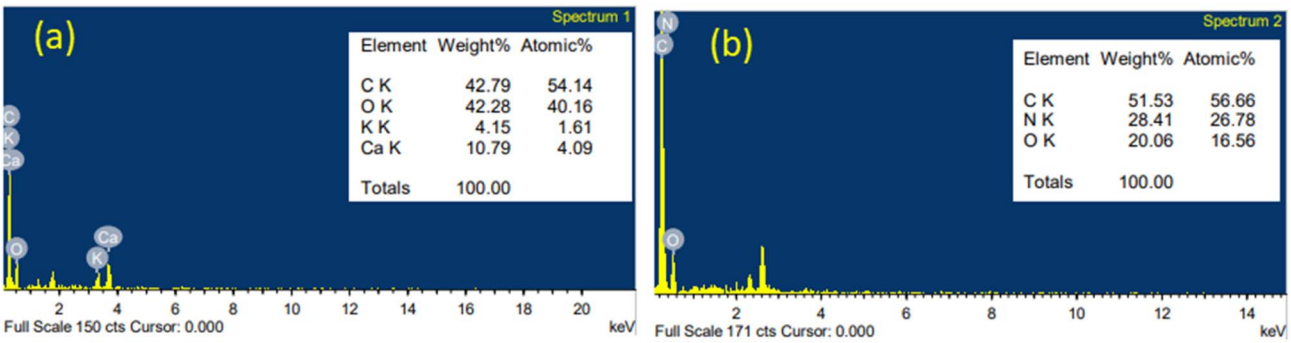

Fig. 5 EDX analysis of ALB (a) and PANI@ALB (b).

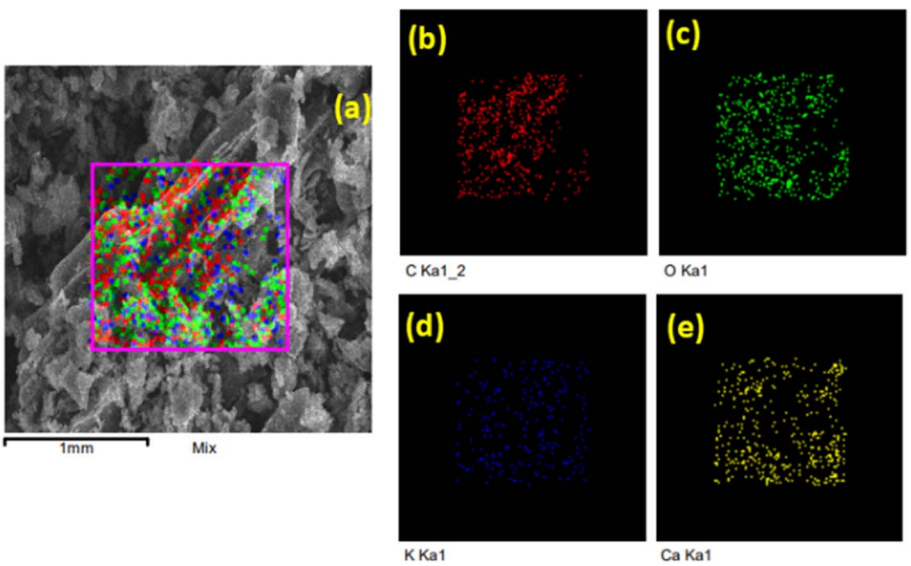

Fig. 6 Elemental mapping of (a) ALB displaying all the elements, (b) mapping of carbon, (c) mapping of oxygen, (d) mapping of potassium, and (e) mapping of calcium.

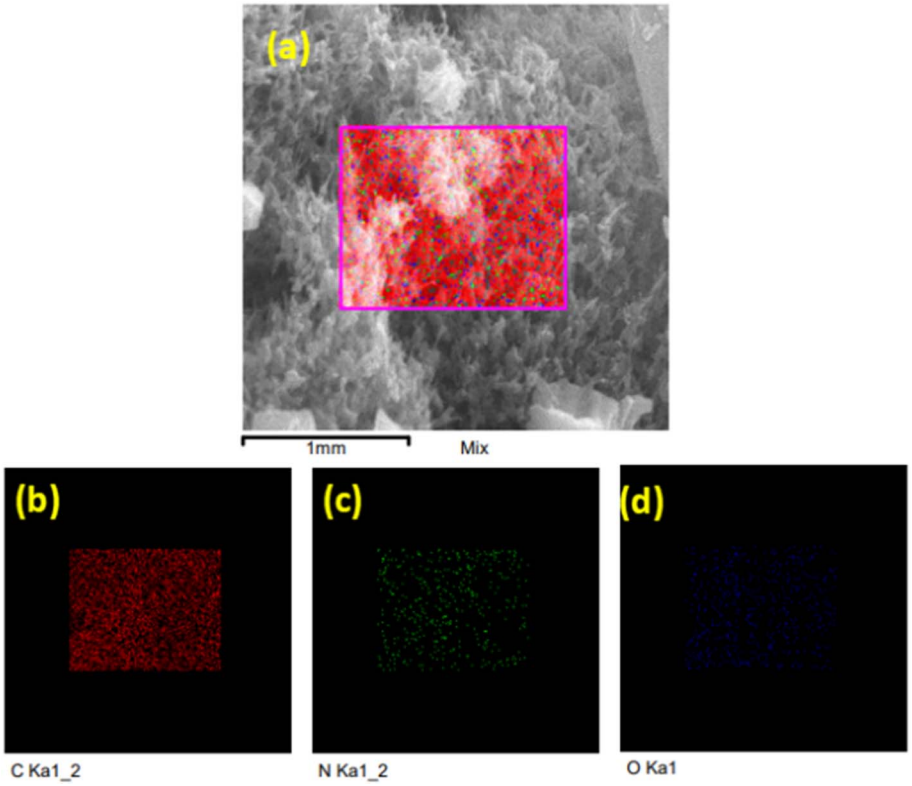

Fig. 7 Elemental mapping of (a) PANI@ALB displaying all the elements, (b) mapping of carbon, (c) mapping of nitrogen, and (d) mapping of oxygen.

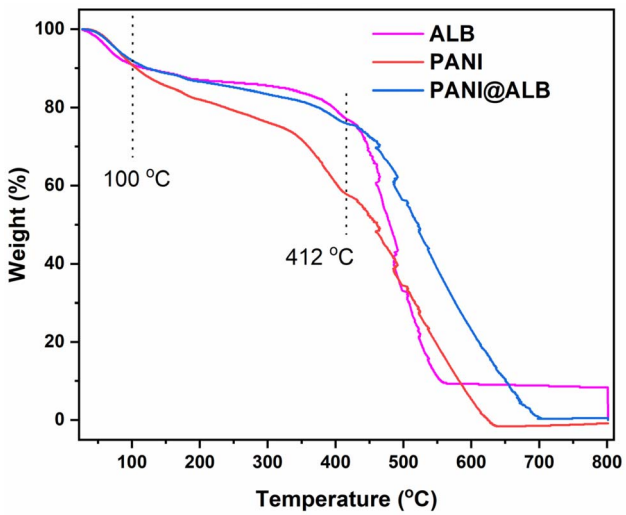

Fig. 8 TG analysis of ALB, PANI, and PANI@ALB.

Lastly, PANI@ALB also suffered weight loss at ~450 to 700 °C, further affirming that PANI in PANI@ALB interacted with ALB to form a composite material with high thermal stability. Thus, it can be concluded from thermal analysis that the final catalyst was stable up to 400 °C.

3.1.5. BET analysis. The surface characteristics (surface area, pore size, and pore volume) of as-synthesized catalysts were thoroughly analyzed using the BET technique. The surface area of ALB calculated by BET analysis was found to be 245.57 $m^2 g^{-1}$, an essential characteristic feature for excellent catalysts. The surface area was further increased upon intercalation of ALB with PANI and reached 252.8 $m^2 g^{-1}$ (Fig. 9a and b). The average pore size and pore volume of ALB were 19.47 Å and 0.01195 $cm^3 g^{-1}$, respectively. After functionalization with PANI, the pore size and volume increased to 23.99 Å, and 0.0151 $cm^3 g^{-1}$, respectively (Fig. 10). This increase in pore size and volume in the final catalyst was assumed to be due to the synergistic interaction of ALB with PANI, without any aggregation of the distinct phases. The superior efficiency of the catalyst PANI@ALB could be attributed to the presence of highly active catalytic sites, which drastically mobilized the catalytic reactions. This is attributed due to the increase in surface area, pore size, and pore volume of the catalyst, which was significantly enhanced in sharp contrast to pristine biochar.[48]

3.1.6. XPS analysis. An XPS analysis was carried out to determine the chemical composition and subsequent evaluation of the surface electronic states of the catalyst PANI@ALB. As shown (Fig. 11), the presence of C, O, and N elements could be observed, and impurity peaks with reference to other elements were nowhere to be found. The XPS spectrum exhibited a C 1s peak at around 284.8 eV, which could be attributed to sp^2-hybridized carbon. On the other hand, the N 1s spectrum displayed a peak at around 399.7 eV, which can be ascribed to N, NH, and positively charged nitrogen (HN^+),

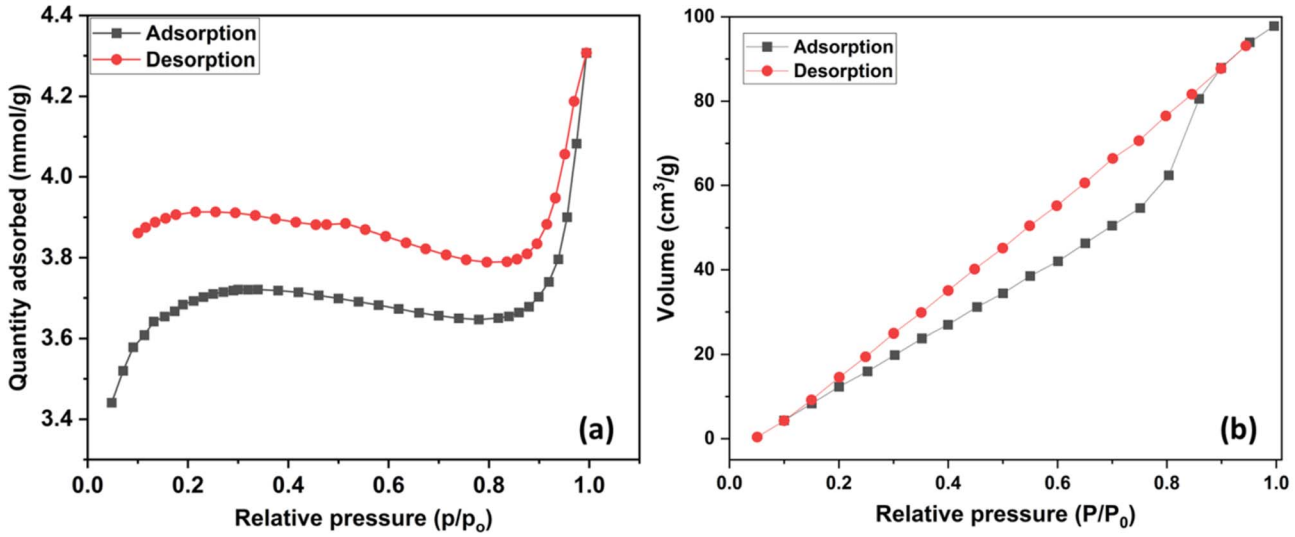

Fig. 9 BET analysis of ALB (a) and the PANI@ALB (b) composite.

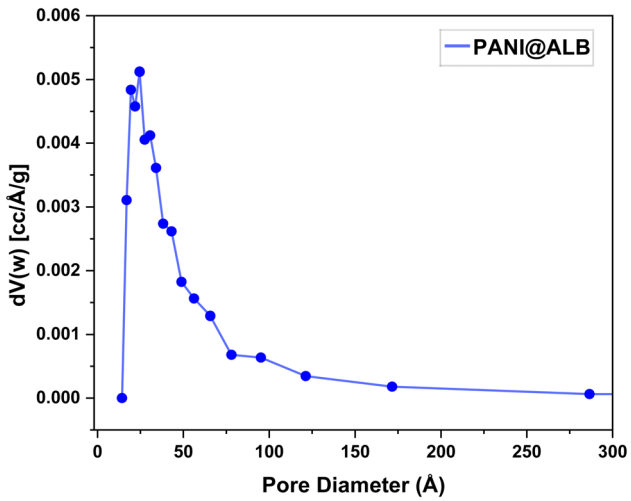

Fig. 10 Pore size distribution of the PANI@ALB catalyst.

respectively. Lastly, a peak of oxygen 1s was observed at around 532.8 eV, which can be attributed to the presence of oxygen atoms of hydroxyl groups.[49] These results highlight the accomplished synthesis of the catalyst PANI@ALB along with its enhanced surface properties and stability.[50,51]

3.2. Investigation of Brønsted acidity of PANI@ALB by the Hammett indicator method

Over the past few decades, spectroscopic approaches have been demonstrated to be effective in assessing the Brønsted acidity of acidic materials.[52,53] Using 4-nitroaniline as an indicator to capture dissociative protons in water, the Hammett indicator method was used to estimate the Brønsted acidity of PANI@ALB.[54] The Brønsted acidity was calculated using the following formula:

$$H_0 = pK(I)_{aq} + \log([I]_s/[IH^+]_s)$$

where H_0 = Hammett acidity function, I = indicator base (4-nitroaniline), $[IH^+]_s$ = molar concentrations of the protonated forms of the indicator, and $[I]_s$ = unprotonated forms of the indicator. To prevent solvent proton influence on the acidity measurement, the experiment for measuring the acidity of PANI@ALB was conducted in an aprotic solvent. The current investigation made use of the previously published value of $pK(I)_{aq}$ for 4-nitroaniline (0.99).[55]

A stock solution of the basic indicator (4-nitroaniline, 10^{-4} mol L^{-1}) was prepared for use throughout the experiment. The absorption spectra of 4-nitroaniline were first recorded using a PerkinElmer UV/VIS Spectrometer Lamda 25 and the absorbance (0.5 a.u.) was measured at 366.86 nm (Fig. 12). Then, 25 mg of ALB and 25 mg of PANI@ALB were added to the freshly prepared 4-nitroaniline solution in two separate flasks and stirred well to make it completely homogeneous. Due to the protonation of the indicator by the Brønsted acidic sites of ALB and the catalyst (PANI@ALB), resulting in the formation of IH^+, the UV-visible spectrum of both mixtures showed a decrease in absorbance, and the maxima were obtained at 0.34 a.u. For both the mixtures, maxima appeared at the same absorbance value, indicating that after functionalization with PANI, acidic sites of ALB remained intact as molecules of PANI either went into the pores of ALB or were present on the surface of ALB. Table 1 summarizes the findings of the calculation of the Hammett acidity function (H_0 = 1.48), which was based on these observations. The findings showed that the material's surface had an adequate number of Brønsted acidic sites.

3.3. Synthesis of heterocycles

3.3.1. Optimization of reaction conditions. The reaction optimization for synthesizing pyranopyrazoles **4** was thoroughly investigated through experiments focusing on catalyst selection, solvent type, temperature, reaction time, and catalyst loading (Table 2). The PANI@ALB catalyst demonstrated

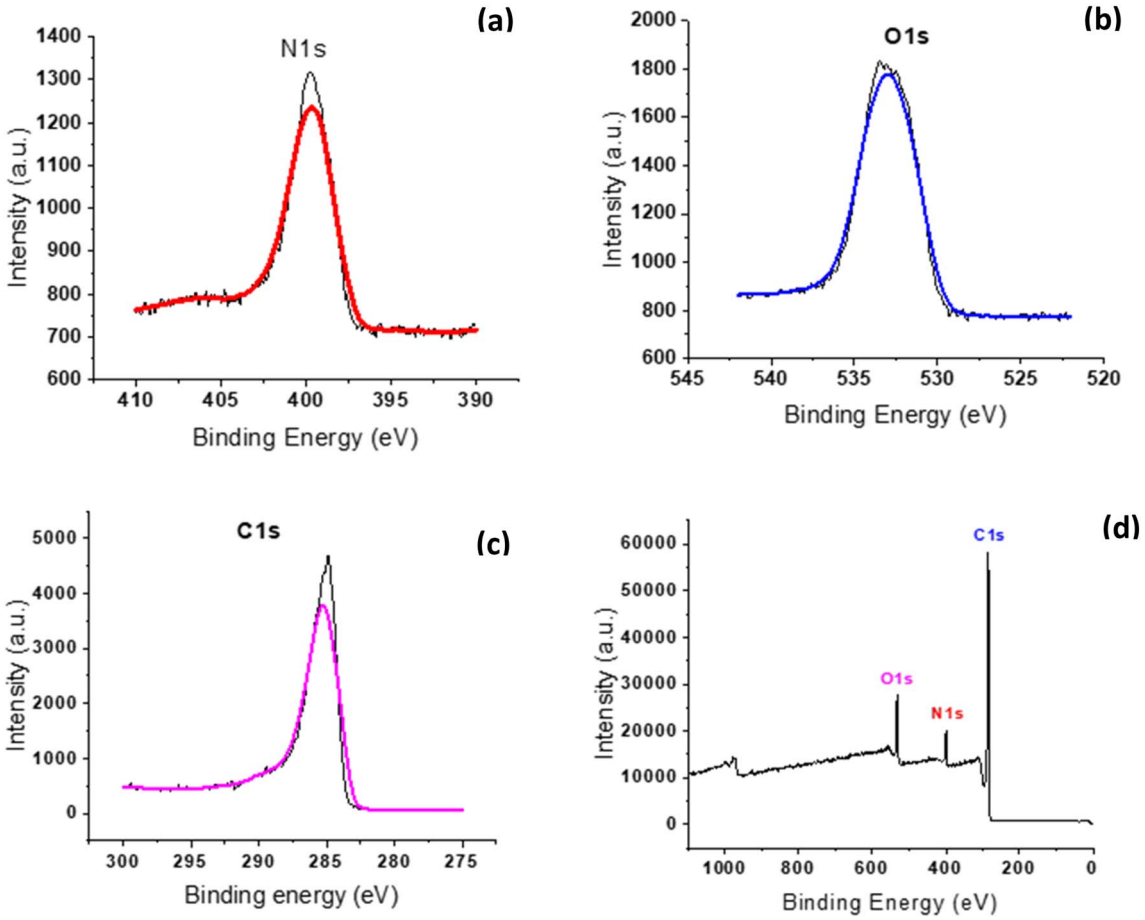

Fig. 11 High-resolution XPS spectrum of (a) N 1s, (b) O 1s, and (c) C 1s, and (d) XPS scan survey spectra of the PANI@ALB catalyst.

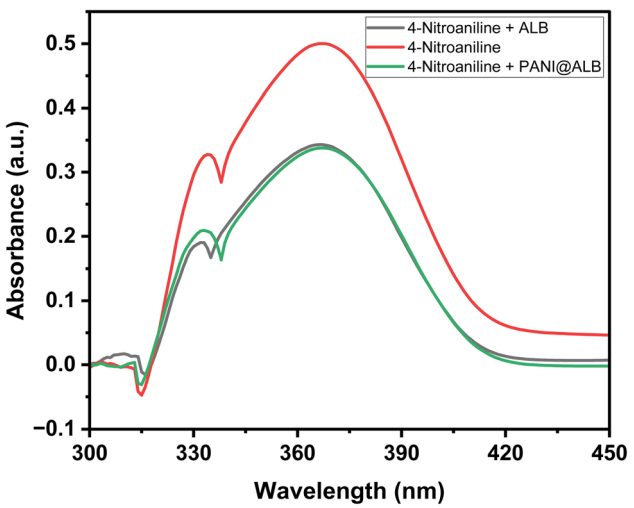

Fig. 12 UV-visible absorption spectra of 4-nitroaniline, a mixture of 4-nitroaniline and ALB, and a mixture of 4-nitroaniline and PANI@ALB.

Table 1 Calculation of H_0 for ALB and PANI@ALB

Entry	Catalyst amount (mg)	A_{max} (a.u.)	$[I]_s$ (%)	$[IH^+]_s$ (%)	H_0
1	None	0.50	100	0	—
2	25	0.34	68	32	1.48
3	25	0.34	68	32	1.48

superior efficacy, achieving a 98% yield in water at 25 °C over 24 hours (Table 2, entry 10).

The reaction was conducted in water as a solvent without a catalyst at 60 °C and 100 °C (increased temperature). At 60 °C, the reaction was completed in 2.5 h, affording a product yield of 45%. Upon increasing the temperature to 100 °C, the product yield was obtained as 48% with a reaction completion time of 2 hours (Table 2, entries 2 and 3). However, when the catalyst (PANI@ALB) was employed, time was reduced, and the yield of the product was enhanced to 98% in 10 minutes at room temperature (25 °C). This acceleration in the rate of the reaction underscores the kinetic advantage imparted by the catalyst by lowering the activation energy barrier. While thermal activation can enhance uncatalyzed reaction rates, it typically requires temperatures above 80–100 °C, consuming more energy and reducing sustainability. The employed catalyst enables the reaction to proceed efficiently at room temperature (25 °C), eliminating the need for external heating.

Table 2 Optimization of reaction conditions[a]

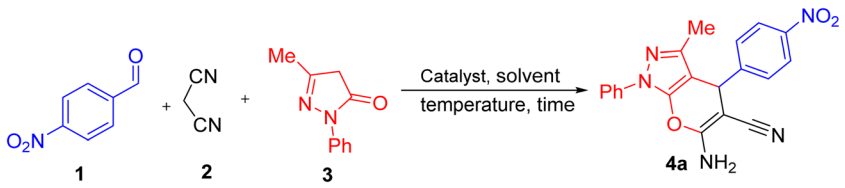

Entry	Catalyst	Catalyst (w/w)%	Solvent	Temp.	Time	Yield of **4a**[b] (%)
1	—	—	H_2O	25 °C	24 h	40
2	—	—	H_2O	60 °C	2.5 h	45
3	—	—	H_2O	100 °C	2 h	48
4	PTSA	15%	H_2O	25 °C	24 h	65
5	Piperidine	15%	H_2O	25 °C	24 h	68
6	DMAP	15%	H_2O	25 °C	24 h	70
7	ALB (2 : 1)	15%	H_2O	25 °C	24 h	82
8	ALB (1 : 1)	15%	H_2O	25 °C	24 h	90
9	PANI	15%	H_2O	25 °C	24 h	88
10	PANI@ALB	15%	H_2O	25 °C	24 h	98
11	PANI@ALB	15%	EtOH	25 °C	24 h	89
12	PANI@ALB	15%	MeOH	25 °C	24 h	79
13	PANI@ALB	15%	ACN	25 °C	24 h	75
14	PANI@ALB	15%	DCM	25 °C	24 h	72
15	PANI@ALB	15%	EtOH : H_2O (1 : 1)	25 °C	24 h	94
16	PANI@ALB	15%	H_2O	25 °C	1h	98
17[c]	**PANI@ALB**	**15%**	**H_2O**	**25°C**	**10 min**	**98**
18	PANI@ALB	15%	H_2O	25 °C	5 min	95
19	PANI@ALB	15%	H_2O	60 °C	10 min	97
20	PANI@ALB	15%	H_2O	100 °C	10 min	98
21	PANI@ALB	5%	H_2O	25 °C	10 min	91
22	PANI@ALB	10%	H_2O	25 °C	10 min	94
23	PANI@ALB	20%	H_2O	25 °C	10 min	97
24	PANI@ALB	25%	H_2O	25 °C	10 min	96

[a] General conditions: **1** (1.0 mmol), **2** (1.0 mmol), **3** (1.0 mmol), and solvent (5.0 mL). [b] Isolated yield after recrystallization in petroleum ether and ethanol. [c] Best reaction conditions.

In summary, we selected this well-known model reaction not because it is intrinsically challenging, but precisely because it provides a rigorous platform to quantitatively and qualitatively validate the efficacy, sustainability, and practicality of the PANI@ALB catalyst.

Compared with alternative catalysts like PANI or ALB alone, which yielded below 90% under similar conditions (entries 5–7), PANI@ALB consistently provided higher yields due to the synergistic effect of both acidic and basic sites, establishing itself as the most efficient and productive catalyst for this reaction. Solvent optimization showed that water outperformed other solvents, with ethanol, methanol, acetonitrile, and dichloromethane yielding 89%, 79%, 75%, and 72%, respectively (Table 2, entries 11–14). This result underlined water as the optimal solvent for maximizing product yield with PANI@ALB. The reaction time optimization revealed that a reduction from 24 hours to just 10 minutes still maintained a high yield (98%) in water (Table 2, entry 17), with only a slight decrease (to 95%) observed when the time was further reduced to 5 minutes (Table 2, entry 18), which indicated that a 10 minute interval was sufficient for the reaction to proceed efficiently. Additionally, temperature optimization studies showed that on increasing the temperature to 100 °C, the reaction was allowed to reach a 98% yield within 10 minutes (Table 2, entry 20), and the reaction achieved the same yield at 25 °C in the same timeframe, indicating that 25 °C is sufficient for optimal efficiency. These findings highlighted that there is no need to increase the temperature, as the reaction proceeds efficiently at room temperature, thereby minimizing energy consumption without compromising product yield. On account of the loading optimization of the catalyst, it was concluded that a 15% (w/w) loading was considered to be ideal and lower loadings resulted in reduced yield (91% at 5% loading) and minimal change beyond 20% (Table 2, entry 21–24), which suggested that 15% is an optimal concentration. In conclusion, PANI@ALB represents the optimized conditions with the catalyst in water at a temperature of 25 °C for a 10 minute duration (Table 2, entry 17), providing a high-yielding, efficient, yet reproducible method for synthesizing pyranopyrazole derivatives (**4**).

3.3.2. Synthesis of pyranopyrazoles 4. Scheme 2 outlines the synthesis of pyranopyrazole derivatives (products **4b** to **4g**) utilizing the optimized reaction conditions by the reaction of various aldehydes (**1**) with malononitrile (**2**) and pyrazolone (**3**). The yields observed with these reactions illustrate the influence of electronic substituents on the aldehyde. Aldehydes possessing

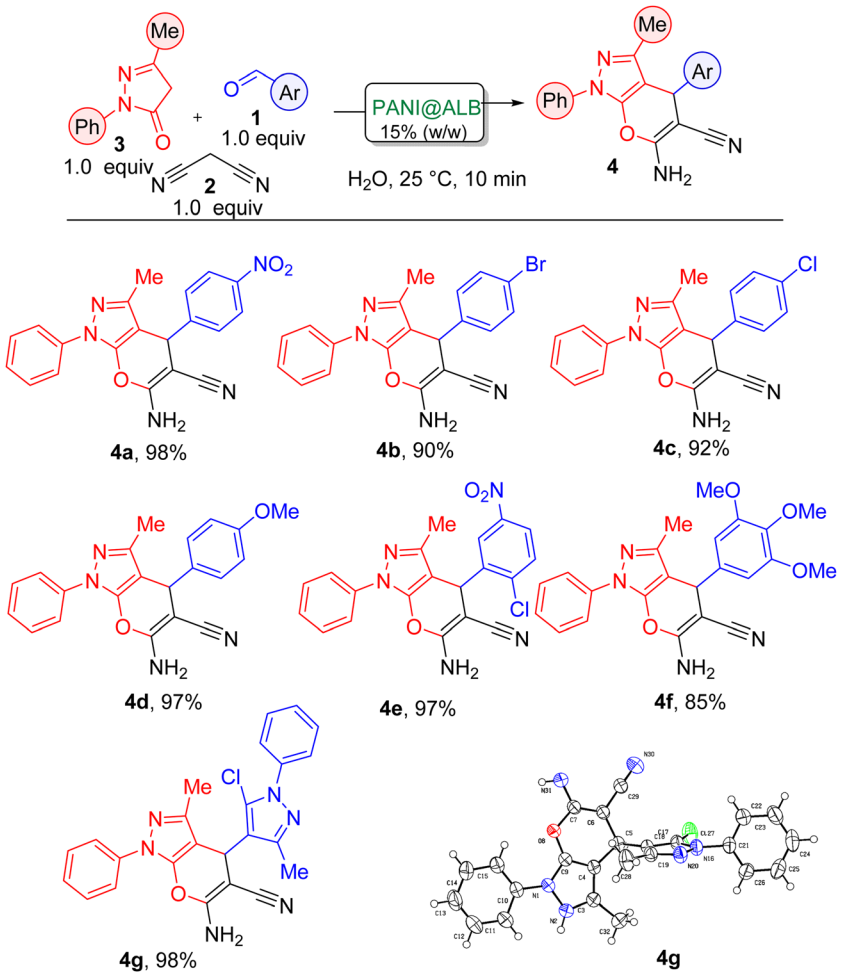

Scheme 2 Synthesis of pyranopyrazoles[a]. [a]Yields mentioned are isolated after recrystallization in petroleum ether and ethanol. E-factor (0.02–0.17). E-factor = (mass of waste/mass of the final product). The CCDC reference number for **4g** is 2416550.

electron-withdrawing substituents, such as 4-bromobenzaldehyde (yielding **4b** with 90%) and 4-chlorobenzaldehyde (yielding **4c** with 92%), exhibited quintessential yields, which indicated that the electron-deficient aldehydes contributed significantly towards the reaction's efficacy. Conversely, aldehydes with electron-donating groups like 4-methoxybenzaldehyde (yielding **4d** with 87%) and 3,4,5-trimethoxybenzaldehyde (yielding **4f** with 85%) resulted in a relatively lower yield, which

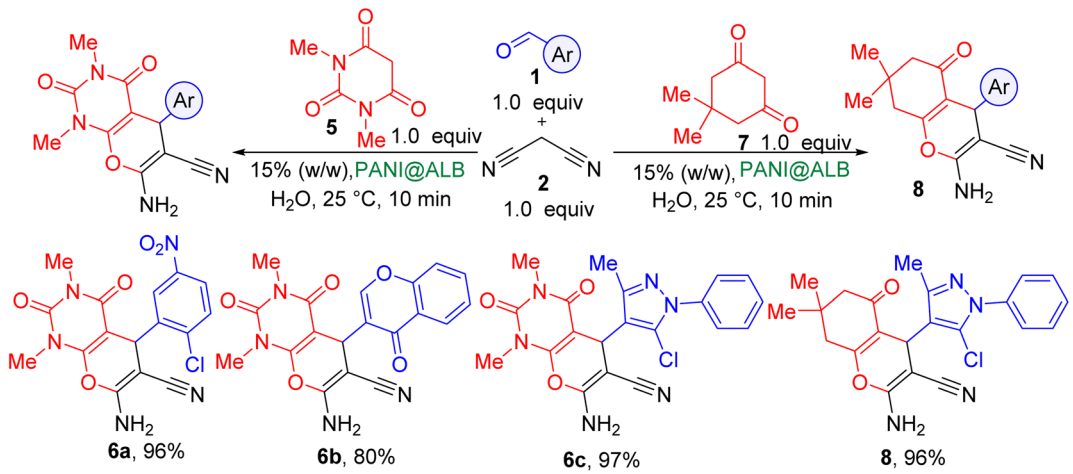

Scheme 3 Synthesis of pyrimidine-fused tetrahydropyrans and tetrahydro-4*H*-chromenes[a]. [a]Yields given were isolated after recrystallization in petroleum ether and ethanol. E-factor (0.04–0.25). E-factor = (mass of waste)/mass of the final product.

suggested that the electron-donating groups might have reduced the Knoevenagel condensation of aldehydes with malononitrile (**2**). A heterocyclic aldehyde, substituted pyrazole carbaldehyde (yielding **4g** with 98%), produced outstanding yields yet again, explicitly implying that the heterocyclic cores are compatible with this reaction.

Furthermore, the single-crystal X-ray diffraction analysis reaffirmed the structure of **4g**. Overall, the entire scheme demonstrated that the optimized conditions using PANI@ALB are particularly well suited for the electron-deficient aldehydes, which further proved the highly efficient synthesis of pyranopyrazoles.

3.3.3. Synthesis of pyrimidine-fused tetrahydropyrans and tetrahydro-4*H*-chromenes. Scheme 3 further extends the scope of the optimized reaction conditions to the synthesis of pyrimidine-fused tetrahydropyran derivatives (products **6a** to **6c**) by reacting aldehydes (**1**) with malononitrile (**2**) and 1,3-dimethylbarbituric acid (**5**). Similar to Scheme 2, electron-withdrawing substituents on aldehydes improved yields, as seen with 2-chloro-5-nitrobenzaldehyde (yielding **6a** with 96%). When a heterocyclic aldehyde like 4-oxo-4*H*-chromene-3-carbaldehyde was utilized, the yield decreased slightly to 80% (yielding **6b**), which strongly implied that the heterocyclic compounds lacking strong electron-withdrawing groups may be less reactive. Substituted pyrazole carbaldehyde (yielding **6c** with 97%) provided an excellent yield yet again, which suggested that the PANI@ALB catalyst is indeed flexible for heterocyclic aldehydes without reductions in yield. This further reinforced that the aldehydes with electron-withdrawing groups perform optimally in synthesizing pyrimidine-fused products.

The scheme also utilized PANI@ALB to synthesize tetrahydro-4*H*-chromene derivatives using aldehydes (**1**), malononitrile (**2**), and dimedone (**7**). This reaction yielded product **8** in a 96% yield, demonstrating that the PANI@ALB catalyst is effective for producing chromene frameworks without compromising yield compared to the reactions in Scheme 2. This unusually high yield suggests that the reaction conditions are adaptable for synthesizing tetrahydro-4*H*-chromenes. Overall, this scheme affirms the adaptability of the conditions to different heterocyclic targets, underlining the method's tremendous versatility.

3.3.4. Plausible mechanism showing bifunctionality of PANI@ALB. Based on the outcomes and preliminary findings that suggested the presence of both Brønsted acidic and Brønsted basic sites in the catalyst, a plausible mechanism for synthesizing the fused heterocycles **4**, **6**, and **8** (Scheme 4) is proposed. Initially, the catalyst coordinated aldehyde **1** probably underwent a PANI@ALB-catalysed Knoevenagel condensation reaction.

Using basic amino groups of PANI with malononitrile **2** *in situ* generated conjugated nitrile intermediate **I**.[56] Concurrently, carbonyl compounds **II** *via* tautomerism participated in a Michael addition reaction catalysed by acidic functionalities of ALB with conjugated nitrile **I**, which in turn produced adduct **III**. This adduct underwent PANI@ALB-assisted intramolecular cyclization to form a six-membered dihydropyran ring (**IV**), which further underwent spontaneous PANI@ALB-assisted tautomerization to yield the final products **4**, **6**, or **8**. The mechanism shown in Scheme 4 has been proposed using previous literature.[57] The relevant intermediates have not been experimentally detected for verification.

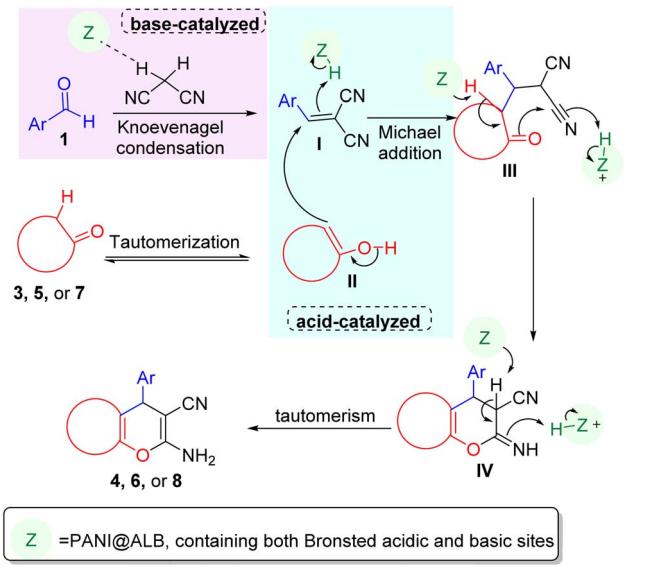

Scheme 4 Plausible mechanism for PANI@ALB-catalyzed synthesis of fused heterocycles (**4**, **6**, and **8**).

3.4. Comparison of the catalytic performance of PANI@ALB with other catalysts

The supremacy of the PANI@ALB catalyst for the synthesis of pyranopyrazoles was also confirmed by comparing its catalytic performance with that of the reported catalysts (Table 3). The

Table 3 Catalytic activity comparison of PANI@ALB with previously published studies

Sr. no.	Catalyst	Reaction conditions	Time	Yield (%)	Reference
1	Salphanilic acid	aq. ethanol, ultrasound	30–60 min	91	58
2	Magnesium oxide	Acetonitrile, reflux	22 min	95	59
3	BAILs (SSA@BAILs)	Neat, 120 °C	15 min	95	60
4	2,5-Furandione, polymer with ethenylbenzene and 1,3,5-triazine-2,4,6-triamine	Ethanol, water, 80 °C	25 min	94	61
5	[BMIm]Br	Water, 80 °C	40 min	96	62
6	**PANI@ALB**	**Water, room temperature**	**10 min**	**98**	**This work**

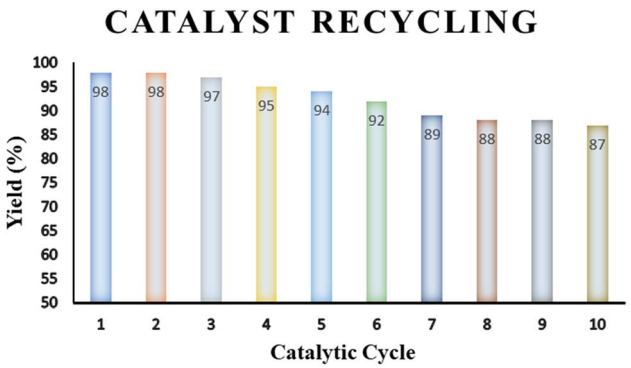

Fig. 13 Study depicting excellent recycling efficiency of the PANI@ALB catalyst after ten cycles on model reaction.

highest yield of the synthesized compounds (98%) in a very short reaction period (10 min) was observed in the presence of the PANI@ALB catalyst (Table 3, entry 6).

3.5. Recycling study of the catalyst

A recyclability study of the catalyst was conducted using a reaction involving 4-nitrobenzaldehyde **1**, malononitrile **2**, and pyrazolone **3** in water at 25 °C, with 15% (w/w) PANI@ALB as the catalyst, aimed at efficient synthesis of pyranopyrazole **4a**. Upon completion, the reaction mixture was immediately filtered utilizing a Buchner funnel, which resulted in a blend of the catalyst and product. Thereafter, ethanol/chloroform (3 : 1 v/v) was added three times to filter and wash this mixture for each cycle, facilitating easy separation and removal of adsorbed organic residual products from the catalyst surface through lucid filtration. The crude product was further purified by recrystallization using a petroleum ether and ethanol mixture. The recovered catalyst was dried at 100 °C, and reused for subsequent cycles. This process was repeated ten times, demonstrating the catalyst's excellent recyclability with negligible reduction in product yield across multiple cycles (Fig. 13). It was inferred from recyclability tests that PANI@ALB maintained high catalytic efficiency, with an initial yield of 98%, slightly reducing to 87% by the 10th cycle. This slight reduction in the efficiency is attributed to the strong adsorption of reactants and residual products on the surface of the catalyst.[63]

FTIR, PXRD, and TG analyses assessed the catalyst's structural stability post-recycling. After the first and tenth cycles, the FTIR spectra of recycled PANI@ALB exhibited bands in nearly identical regions as those of fresh PANI@ALB, confirming its functional group retention and chemical stability (Fig. 14). Additionally, the PXRD analysis of fresh, first, and tenth recycled catalysts showed retention of major peaks observed at 9.1°,15.3°, 20.6°, and 25.3°, confirming structural stability of the catalyst after multiple cycles of reuse (Fig. 15). TG analysis of fresh and recycled catalysts also revealed that no thermal changes occurred in the structural framework during the catalytic reaction (Fig. S1). These findings reaffirmed that PANI@ALB possesses immensely high catalytic efficiency and excellent reusability, while maintaining the structural integrity of the catalyst throughout the complete process.

3.6. Green metrics

The environmental benignity of the reactions employed throughout the study was evaluated *via* assessment of varied parameters, including the E-factor, atom economy, yield, and

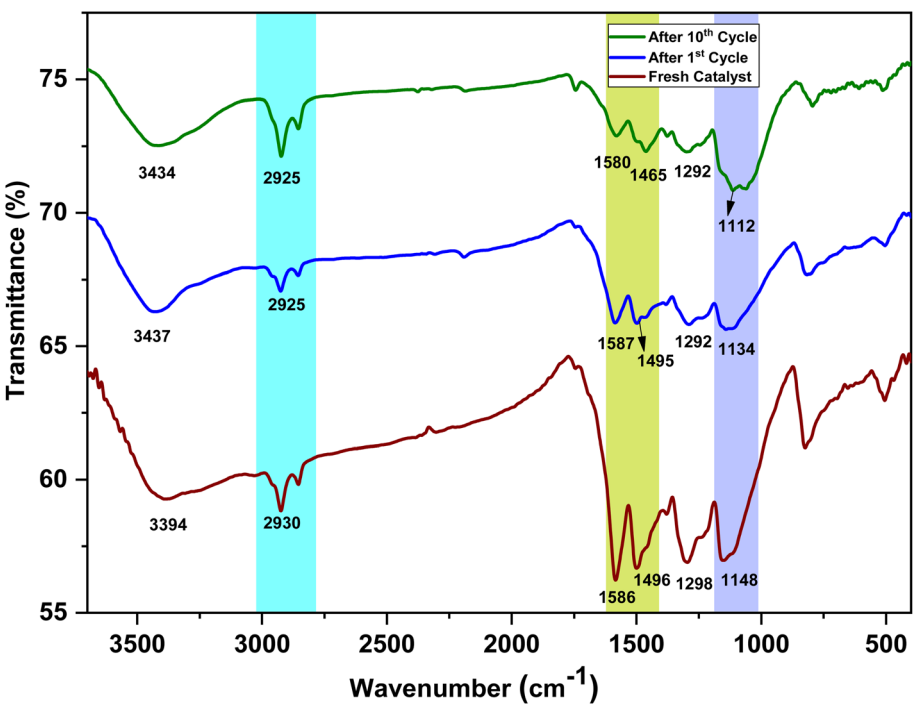

Fig. 14 FT-IR spectra of the fresh catalyst, and the catalyst after the first cycle and the tenth cycle.

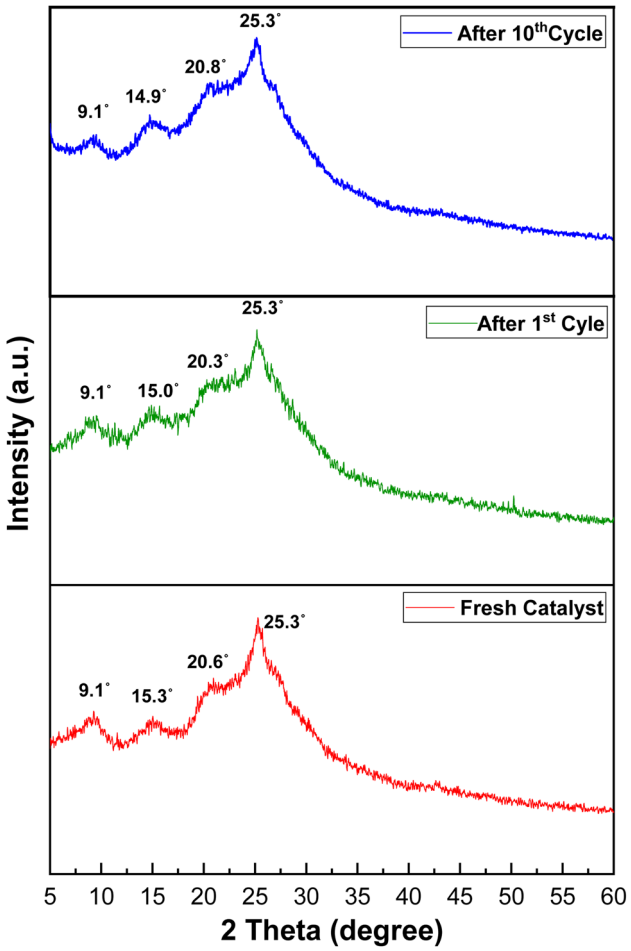

Fig. 15 XRD spectra of the fresh catalyst, and the catalyst after the first cycle and the tenth cycle.

catalyst activity. Notably, it was found that the reaction showed E-factors in the range of 0.02–0.25, which denoted that the reaction produced a minimal amount of waste, which was also affirmed by the calculation of atom economy (around 95%). The catalyst also exhibited remarkable efficiency with high TOF in the range of 71.39–90.7. This protocol exhibited tremendously high yields while maintaining high efficiency, yet in relatively short reaction times.

4 Conclusion

In light of an upsurge in environmentally detrimental catalysts, an orchestrated PANI@ALB hybrid composite synthesized by *in situ* chemical oxidative polymerization of aniline on activated lac tree biochar is a novel acid–base bifunctional heterogeneous catalyst for the synthesis of pyranopyrazoles, pyrimidine-fused tetrahydropyrans, and tetrahydro-4*H*-chromene derivatives. The catalyst exceeded expectations with high yields, E-factor (0.02–0.25), atom economy (95%), turnover numbers, and eco-compatibility, and improved recyclability. We propose the PANI@ALB hybrid composite as a highly productive setup for synthesizing fused pharmacologically relevant heterocyclic moieties, expanding the horizon for biochar-based functional nanomaterials, and a sustainable platform for carbon materials.

Author contributions

Nida Khan conducted the experiments, compound characterization, and data analysis, and drafted the manuscript. Mo Shadab and M. B. Siddiqui provided the leaves of *Schleichera oleosa*. Mohd Umar Khan assisted with the software, and Zeba N. Siddiqui supervised the study and edited the final draft.

Conflicts of interest

The authors declare no competing financial interests.

Data availability

The data supporting this article have been included as part of the SI. Appendix A: (1) General information, (1.1) Materials, (1.2) Physical methods; appendix B: (2) Experimental section, (2.1) Collection of Kusum leaves, (2.2) Washing of leaves, (2.3) Drying of leaves, (2.4) Grinding of the dried leaves, (2.5) General procedure for the synthesis of pyrazole-fused dihydropyrans **4**, pyrimidine-fused tetrahydropyrans **6** and tetrahydro-4*H*-chromenes **8**; appendix C: (3) Characterization data and corresponding spectra of compounds, (3.1) Characterisation data of synthesized compounds: **4a–4h**, **6a–6c**, **8**, and **12a–12j**, (3.2) Single crystal data of compound **4g**: CCDC: 2416550, (3.3) Process-scale organic synthesis, Scheme C1: Gram-scale synthesis of **4a**. Yields given are isolated after recrystallization in petroleum ether and ethanol; appendix D: (4) Recycled data, (4.1) Comparison of TGA of fresh catalyst and recycled catalyst, (4.2) Hot filtration test. See DOI: **https://doi.org/10.1039/d5su00279f**.

CCDC 2416550 (**4g**) contains the supplementary crystallographic data for this paper.[64]

Acknowledgements

The authors want to acknowledge their institutions for their technical and administrative support.

References

1 K. Motokura, M. Tada and Y. Iwasawa, Layered Materials with Coexisting Acidic and Basic Sites for Catalytic One-Pot Reaction Sequences, *J. Am. Chem. Soc.*, 2009, **131**(23), 7944–7945, DOI: **10.1021/ja9012003**.

2 V. Rodionov, H. Gao, S. Scroggins, D. A. Unruh, A. J. Avestro and J. M. J. Fréchet, Easy Access to a Family of Polymer Catalysts from Modular Star Polymers, *J. Am. Chem. Soc.*, 2010, **132**(8), 2570–2572, DOI: **10.1021/ja9104842**.

3 F. Shang, H. Liu, J. Sun, B. Liu, C. Wang, J. Guan and Q. Kan, Synthesis, Characterization and Catalytic Application of Bifunctional Catalyst: Al-MCM-41-NH2, *Catal. Commun.*, 2011, **12**(8), 739–743, DOI: **10.1016/j.catcom.2011.01.010**.

4 H. Li, H. Wu, Q. Zhang, J. Liu, X. Liu, Y. Liu and S. Yang, Solid Acid-Base Bifunctional Catalysts in Organic Transformations, *Curr. Catal.*, 2013, **2**(3), 173–212, DOI: 10.2174/22115447113029990014.

5 W. J. Liu, H. Jiang and H. Q. Yu, Development of Biochar-Based Functional Materials: Toward a Sustainable Platform Carbon Material, *Chem. Rev.*, 2015, **115**(22), 12251–12285, DOI: 10.1021/acs.chemrev.5b00195.

6 X. f. Tan, S. b. Liu, Y. g. Liu, Y. l. Gu, G. m. Zeng, X. j. Hu, X. Wang, S. h. Liu and L. h. Jiang, Biochar as Potential Sustainable Precursors for Activated Carbon Production: Multiple Applications in Environmental Protection and Energy Storage, *Bioresour. Technol.*, 2017, **227**, 359–372, DOI: 10.1016/j.biortech.2016.12.083.

7 Y. Wang, Y. Zhang, L. Pei, D. Ying, X. Xu, L. Zhao, J. Jia and X. Cao, Converting Ni-Loaded Biochars into Supercapacitors: Implication on the Reuse of Exhausted Carbonaceous Sorbents, *Sci. Rep.*, 2017, **7**(1), 41523, DOI: 10.1038/srep41523.

8 J. Lee, K. H. Kim and E. E. Kwon, Biochar as a Catalyst, *Renew. Sustain. Energy Rev.*, 2017, **77**, 70–79, DOI: 10.1016/j.rser.2017.04.002.

9 A. A. Wani, N. Shaari, A. A. Ansari, S. Mohd, P. Tiwari, S. K. Kamarudin and R. K. Gupta, Polyaniline-Based Functional Nanohybrid Materials towards Environmental Remediation; Current Progress, Challenges, and Future Perspectives, *J. Environ. Chem. Eng.*, 2023, **11**(6), 111254, DOI: 10.1016/j.jece.2023.111254.

10 N. Khan, A. Gupta, S. Ahamad, M. K. Hussain, M. U. Khan and Z. N. Siddiqui, Functionalized Biochar Catalysts: Advancing Green Chemistry in Synthesis of O- and N-Heterocycles, *Environ. Res.*, 2025, **284**, 122136, DOI: 10.1016/j.envres.2025.122136.

11 Z. Chen, Q. Li, Y. Xiao, C. Zhang, Z. Fu, Y. Liu, X. Yi, A. Zheng, C. Li and D. Yin, Acid–Base Synergistic Catalysis of Biochar Sulfonic Acid Bearing Polyamide for Microwave-Assisted Hydrolysis of Cellulose in Water, *Cellulose*, 2019, **26**(2), 751–762, DOI: 10.1007/s10570-018-2098-3.

12 J. L. Vidal, V. P. Andrea, S. L. MacQuarrie and F. M. Kerton, Oxidized Biochar as a Simple, Renewable Catalyst for the Production of Cyclic Carbonates from Carbon Dioxide and Epoxides, *ChemCatChem*, 2019, **11**(16), 4089–4095, DOI: 10.1002/cctc.201900290.

13 P. Moradi, M. Hajjami and B. Tahmasbi, Fabricated Copper Catalyst on Biochar Nanoparticles for the Synthesis of Tetrazoles as Antimicrobial Agents, *Polyhedron*, 2020, **175**, 114169, DOI: 10.1016/j.poly.2019.114169.

14 S. Pang, F. Liu, Y. Zhang, Z. Dong, Q. Su, W. Wang, Z. Li, F. Zhou and Y. Wang, Construction of Functional Superhydrophobic Biochars as Hydrogen Transfer Catalysts for Dehydrogenation of N-Heterocycles, *ACS Sustain. Chem. Eng.*, 2021, **9**(27), 9062–9077, DOI: 10.1021/acssuschemeng.1c02322.

15 P. Moradi and M. Hajjami, Magnetization of Biochar Nanoparticles as a Novel Support for Fabrication of Organo Nickel as a Selective, Reusable and Magnetic Nanocatalyst in Organic Reactions, *New J. Chem.*, 2021, **45**(6), 2981–2994, DOI: 10.1039/d0nj04990e.

16 D. Dharmendra, P. Chundawat, Y. Vyas, P. Chaubisa, M. Kumawat and C. Ameta, Eco-Friendly Design of TiO2 Nanoparticles Supported on Fe3O4 Coated Carbon-Based Biochar Substrate for the Synthesis of Pyrano-[2, 3-c]-Pyrazole Derivatives, *Renew. Sustain. Energy Rev.*, 2022, **28**, 100732, DOI: 10.1016/j.scp.2022.100732.

17 S. Z. Zhang, L. N. Dong, L. P. Mo and Z. H. Zhang, Magnetic Biochar-Supported ZrO2 as an Efficient Catalyst for One-Pot Synthesis of 1′,4′-Dihydro-3H,3′H-Spiro[Furo[3,4-b] Quinoline-9,2′-Quinoxaline]-1,3′(4H)-Diones, *Appl. Organomet. Chem.*, 2023, **37**(2), 1–13, DOI: 10.1002/aoc.6949.

18 L. N. Dong, Y. M. Wang, W. L. Zhang, L. P. Mo and Z. H. Zhang, Nickel Supported on Magnetic Biochar as a Highly Efficient and Recyclable Heterogeneous Catalyst for the One-Pot Synthesis of Spirooxindole-Dihydropyridines, *Appl. Organomet. Chem.*, 2022, **36**(5), 1–12, DOI: 10.1002/aoc.6667.

19 L. N. Dong, S. Z. Zhang, W. L. Zhang, Y. Dong, L. P. Mo and Z. H. Zhang, Synthesis, Characterization and Application of Magnetic Biochar Sulfonic Acid as a Highly Efficient Recyclable Catalyst for Preparation of Spiro-Pyrazolo[3,4-b] Pyridines, *Res. Chem. Intermed.*, 2022, **48**(3), 1249–1272, DOI: 10.1007/s11164-022-04660-6.

20 L. Mohammadi, M. M. Heravi, A. Saljooqi and P. Mohammadi, The Preparation of Polyvinyl Imidazole-Functionalized Magnetic Biochar Decorated by Silver Nanoparticles as an Efficient Catalyst for the Synthesis of Spiro-2-Amino-4H-Pyran Compounds, *Sci. Rep.*, 2022, **12**(1), 1–17, DOI: 10.1038/s41598-022-25857-0.

21 M. Norouzi, P. Moradi and M. Khanmoradi, Aluminium-Based Ionic Liquid Grafted on Biochar as a Heterogeneous Catalyst for the Selective Synthesis of Tetrazole and 2,3-Dihydroquinazolin 4(1H)-One Derivatives, *RSC Adv.*, 2023, **13**(50), 35569–35582, DOI: 10.1039/d3ra06440a.

22 M. Borzooei and M. Norouzi, Design, Synthesis, Characterization and Application of Magnetic Biochar as a Reusable Nano Catalyst for the Synthesis of Tetrazole Derivatives, *Colloid Nanosci. J.*, 2023, **1**(4), 173–181, DOI: 10.61186/cnj.1.4.173.

23 D. Dharmendra, P. Chundawat, Y. Vyas, P. Chaubisa and C. Ameta, Greener Design and Characterization of Biochar/Fe3O4@SiO2-Ag Magnetic Nanocomposite as Efficient Catalyst for Synthesis of Bioactive Benzylpyrazolyl Coumarin Derivatives, *RSC Adv.*, 2023, **13**(21), 14594–14613, DOI: 10.1039/d3ra00869j.

24 N. Emad-Abbas, J. Naji, P. Moradi and T. Kikhavani, 3-(Sulfamic Acid)-Propyltriethoxysilane on Biochar Nanoparticles as a Practical, Biocompatible, Recyclable and Chemoselective Nanocatalyst in Organic Reactions, *RSC Adv.*, 2024, **14**(31), 22147–22158, DOI: 10.1039/d4ra02265c.

25 M. M. Maseer, T. Kikhavani and B. Tahmasbi, A Multidentate Copper Complex on Magnetic Biochar Nanoparticles as a Practical and Recoverable Nanocatalyst for the Selective Synthesis of Tetrazole Derivatives,

Nanoscale Adv., 2024, **6**(15), 3948–3960, DOI: **10.1039/d4na00284a**.

26 B. Tahmasbi, P. Moradi and M. Darabi, A New Neodymium Complex on Renewable Magnetic Biochar Nanoparticles as an Environmentally Friendly, Recyclable and Efficient Nanocatalyst in the Homoselective Synthesis of Tetrazoles, *Nanoscale Adv.*, 2024, 1932–1944, DOI: **10.1039/d3na01087b**.

27 D. Khalili, A. A. Ramjerdi, H. R. Boostani and A. Ghaderi, Biochar: A High Performance and Renewable Basic Carbocatalyst for Facilitating Room Temperature Synthesis of 4H-Benzo[h]Chromene and Pyranopyrazoles in Water, *Biochar*, 2024, **6**(1), 6, DOI: **10.1007/s42773-023-00286-y**.

28 M. Alekasir, S. Heydarian and B. Tahmasbi, The Synthesis of Biochar from Biomass Waste Recycling and Its Surface Modification for Immobilization of a New Cu Complex as a Reusable Nanocatalyst in the Homoselective Synthesis of Tetrazoles, *Res. Chem. Intermed.*, 2024, **50**(5), 2031–2049, DOI: **10.1007/s11164-024-05252-2**.

29 A. K. Yadav, N. Mohammad, E. Chamanehpour, Y. K. Mishra and P. K. Khanna, Polyaniline (PANI) Nanocomposites with Se, Te and Their Metal Chalcogenides: A Review, *RSC Appl. Polym.*, 2024, **2**(5), 775–794, DOI: **10.1039/d4lp00093e**.

30 S. Z. Zhang, Z. S. Cui, M. Zhang and Z. H. Zhang, Biochar-Based Functional Materials as Heterogeneous Catalysts for Organic Reactions, *Curr. Opin. Green Sustainable Chem.*, 2022, **38**, 100713, DOI: **10.1016/j.cogsc.2022.100713**.

31 A. Baitha, A. Gopinathan, K. Krishnan and V. V. Dabholkar, Synthesis of 2-Amino-4-(2-Ethoxybenzo[d][1,3]Dioxol-5-Yl)-4H-Pyran-3-Carbonitrile Derivatives and Their Biological Evaluation, *J. Heterocycl. Chem.*, 2018, **55**(5), 1189–1192, DOI: **10.1002/jhet.3152**.

32 W. Kemnitzer, J. Drewe, S. Jiang, H. Zhang, J. Zhao, C. Crogan-Grundy, L. Xu, S. Lamothe, H. Gourdeau, R. Denis, B. Tseng, S. Kasibhatla and X. C. Sui, Discovery of 4-Aryl-4H-Chromenes as a New Series of Apoptosis Inducers Using a Cell- and Caspase-Based High-Throughput Screening Assay. 3. Structure-Activity Relationships of Fused Rings at the 7,8-Positions, *J. Med. Chem.*, 2007, **50**(12), 2858–2864, DOI: **10.1021/jm070216c**.

33 G. Zhang, Y. Zhang, J. Yan, R. Chen, S. Wang, Y. Ma and R. Wang, One-Pot Enantioselective Synthesis of Functionalized Pyranocoumarins and 2-Amino-4 H -Chromenes: Discovery of a Type of Potent Antibacterial Agent, *J. Org. Chem.*, 2012, **77**(2), 878–888, DOI: **10.1021/jo202020m**.

34 M. N. Erichsen, T. H. V. Huynh, B. Abrahamsen, J. F. Bastlund, C. Bundgaard, O. Monrad, A. Bekker-Jensen, C. W. Nielsen, K. Frydenvang, A. A. Jensen and L. Bunch, Structure-Activity Relationship Study of First Selective Inhibitor of Excitatory Amino Acid Transporter Subtype 1: 2-Amino-4-(4-Methoxyphenyl)-7-(Naphthalen-1-Yl)-5-Oxo-5,6,7,8-Tetrahydro-4 H -Chromene-3-Carbonitrile (UCPH-101), *J. Med. Chem.*, 2010, **53**(19), 7180–7191, DOI: **10.1021/jm1009154**.

35 R. Kaur, F. Naaz, S. Sharma, S. Mehndiratta, M. K. Gupta, P. M. S. Bedi and K. Nepali, Screening of a Library of 4-Aryl/Heteroaryl-4H-Fused Pyrans for Xanthine Oxidase Inhibition: Synthesis, Biological Evaluation and Docking Studies, *Med. Chem. Res.*, 2015, **24**(8), 3334–3349, DOI: **10.1007/s00044-015-1382-0**.

36 S. Wang, L. Ren, Y. Liu, Z. Han and Y. Yang, Mechanical Characteristics of Typical Plant Leaves, *J. Bionic Eng.*, 2010, **7**(3), 294–300, DOI: **10.1016/S1672-6529(10)60253-3**.

37 H. Guleria and M. Vaidya, Anatomical Studies of *Schleichera oleosa* (Lour.) Oken, *World J. Pharm. Res.*, 2015, **4**(12), 1178–1188.

38 S. Anto, M. P. Sudhakar, T. Shan Ahamed, M. S. Samuel, T. Mathimani, K. Brindhadevi and A. Pugazhendhi, Activation Strategies for Biochar to Use as an Efficient Catalyst in Various Applications, *Fuel*, 2021, **285**, 119205, DOI: **10.1016/j.fuel.2020.119205**.

39 S. Siddiqui and Z. N. Siddiqui, Copper Schiff Base Functionalized Polyaniline (Cu-SB/PANI): A Highly Efficient Polymer Based Organometallic Catalyst for the Synthesis of 2-Amino Chromene Derivatives, *Appl. Organomet. Chem.*, 2019, **33**(10), e5161, DOI: **10.1002/aoc.5161**.

40 F. Tomassoni, E. E. Schneider, C. L. Giroletti, M. E. Nagel-Hassemer, M. A. L. Recio and F. R. Lapolli, Production and Characterization of Activated Biochar of Cássia Fistula L. Leaves, *Environ. Manag. Sustain. Magazine*, 2020, **9**, 800–815, DOI: **10.19177/rgsa.v9e02020800-815**.

41 M. L. Yeboah, X. Li and S. Zhou, Facile Fabrication of Biochar from Palm Kernel Shell Waste and Its Novel Application to Magnesium-Based Materials for Hydrogen Storage, *Materials*, 2020, **13**(3), 625, DOI: **10.3390/ma13030625**.

42 Y. Liu, X. Zhao, J. Li, D. Ma and R. Han, Characterization of Bio-Char from Pyrolysis of Wheat Straw and Its Evaluation on Methylene Blue Adsorption, *Desalin. Water Treat.*, 2012, **46**(1–3), 115–123, DOI: **10.1080/19443994.2012.677408**.

43 B. Sydulu Singu, P. Srinivasan and S. Pabba, Benzoyl Peroxide Oxidation Route to Nano Form Polyaniline Salt Containing Dual Dopants for Pseudocapacitor, *J. Electrochem. Soc.*, 2011, **159**(1), A6–A13, DOI: **10.1149/2.036201jes**.

44 S. Padmapriya, S. Harinipriya, K. Jaidev, V. Sudha, D. Kumar and S. Pal, Storage and Evolution of Hydrogen in Acidic Medium by Polyaniline, *Int. J. Energy Res.*, 2018, **42**(3), 1196–1209, DOI: **10.1002/er.3920**.

45 S. Wang, C. Zhao, R. Shan, Y. Wang and H. Yuan, A Novel Peat Biochar Supported Catalyst for the Transesterification Reaction, *Energy Convers. Manag.*, 2017, **139**, 89–96, DOI: **10.1016/j.enconman.2017.02.039**.

46 M. Hosny, M. Fawzy and A. S. Eltaweil, Green Synthesis of Bimetallic Ag/ZnO@Biohar Nanocomposite for Photocatalytic Degradation of Tetracycline, Antibacterial and Antioxidant Activities, *Sci. Rep.*, 2022, **12**(1), 7316, DOI: **10.1038/s41598-022-11014-0**.

47 Y. Qing, X. Wang, Y. Wang, X. Yang, Z. Yang and L. Yang, Study on In-Situ Polymerization of PANI/APP and Its Application in HDPE, *Polym. Bull.*, 2018, **75**(1), 345–370, DOI: **10.1007/s00289-017-2034-y**.

48 M. P. Schmidt, D. J. Ashworth, N. Celis and A. M. Ibekwe, Optimizing Date Palm Leaf and Pistachio Shell Biochar

Properties for Antibiotic Adsorption by Varying Pyrolysis Temperature, *Bioresour. Technol. Rep.*, 2023, **21**, 101325, DOI: 10.1016/j.biteb.2022.101325.

49 C. Peiris, S. R. Gunatilake, T. E. Mlsna, D. Mohan and M. Vithanage, Biochar Based Removal of Antibiotic Sulfonamides and Tetracyclines in Aquatic Environments: A Critical Review, *Bioresour. Technol.*, 2017, **246**, 150–159, DOI: 10.1016/j.biortech.2017.07.150.

50 S. Ge, S. Wang, W. Mai, K. Zhang, M. Tanveer, L. Wang and C. Tian, Characteristics and Acidic Soil Amelioration Effects of Biochar Derived from a Typical Halophyte Salicornia Europaea L. (Common Glasswort), *Environ. Sci. Pollut. Res.*, 2023, **30**(24), 66113–66124, DOI: 10.1007/s11356-023-27182-z.

51 M. Li, W. Yin, X. Han and X. Chang, Hierarchical Nanocomposites of Polyaniline Scales Coated on Graphene Oxide Sheets for Enhanced Supercapacitors, *J. Solid State Electrochem.*, 2016, **20**(7), 1941–1948, DOI: 10.1007/s10008-016-3202-y.

52 C. Thomazeau, H. Olivier-Bourbigou, L. Magna, S. Luts and B. Gilbert, Determination of an Acidic Scale in Room Temperature Ionic Liquids, *J. Am. Chem. Soc.*, 2003, **125**(18), 5264–5265, DOI: 10.1021/ja0297382.

53 Z. Duan, Y. Gu, J. Zhang, L. Zhu and Y. Deng, Protic Pyridinium Ionic Liquids: Synthesis, Acidity Determination and Their Performances for Acid Catalysis, *J. Mol. Catal. A:Chem.*, 2006, **250**(1–2), 163–168, DOI: 10.1016/j.molcata.2006.01.035.

54 H. Xing, T. Wang, Z. Zhou and Y. Dai, The Sulfonic Acid-Functionalized Ionic Liquids with Pyridinium Cations: Acidities and Their Acidity-Catalytic Activity Relationships, *J. Mol. Catal. A:Chem.*, 2007, **264**(1–2), 53–59, DOI: 10.1016/j.molcata.2006.08.080.

55 F. Parveen, T. Patra and S. Upadhyayula, Hydrolysis of Microcrystalline Cellulose Using Functionalized Bronsted Acidic Ionic Liquids - A Comparative Study, *Carbohydr. Polym.*, 2016, **135**, 280–284, DOI: 10.1016/j.carbpol.2015.08.039.

56 H. Tian, S. Liu, Z. Zhang, T. Dang, Y. Lu and S. Liu, Highly Stable Polyoxovanadate-Based Zn-MOF with Dual Active Sites as a Solvent-Free Catalyst for C-C Bond Formation, *ACS Sustain. Chem. Eng.*, 2021, **9**(12), 4660–4667, DOI: 10.1021/acssuschemeng.1c00389.

57 S. Samai, S. Atta and M. S. Singh, Synthetic Strategies Toward 2H-, 4H-Pyrans, and Pyranones: Recent Advances, *ChemistrySelect*, 2025, **10**(21), 01023, DOI: 10.1002/slct.202501023.

58 P. J. Patel, H. R. Chaudhary, V. K. Gupta and D. M. Patel, Correction to: Sonochemical Synthesis of Benzylidene Derivatives of Enolizable Carbonyls and Their Analogues in Aqueous Ethanol, *Res. Chem. Intermed.*, 2024, **50**(4), 1941–1943, DOI: 10.1007/s11164-024-05233-5.

59 H. Sheibani and M. Babaie, Three-Component Reaction to Form 1,4-Dihydropyrano[2,3-c]Pyrazol-5-Yl Cyanides, *Synth. Commun.*, 2010, **40**(2), 257–265, DOI: 10.1080/00397910902964866.

60 N. Iravani, M. Keshavarz and L. A. Taib, Acidic Ionic Liquids Immobilized on Nano Silica Sulfuric Acid for Highly Effective Catalytic Synthesis of 4H-Pyrano[2,3-c]Pyrazole and Dihydropyrano[c]Chromene Derivatives, *Res. Chem. Intermed.*, 2023, **49**(10), 4405–4422, DOI: 10.1007/s11164-023-05105-4.

61 F. Ghorbanipour, S. M. Nezhad, S. A. Pourmousavi, E. N. Zare and G. Heidari, Superparamagnetic Polymer Nanocomposite as a Catalyst for the Synthesis of Pyrano[3,2-c]Chromene, Pyrano[2,3-c]Pyrazole, and Benzylpyrazolyl Coumarin, *Inorg. Chem. Commun.*, 2023, **147**, 110271, DOI: 10.1016/j.inoche.2022.110271.

62 S. Chakraborty, B. Paul, U. C. De, R. Natarajan and S. Majumdar, Water-SDS-[BMIm]Br Composite System for One-Pot Multicomponent Synthesis of Pyrano[2,3-c] Pyrazole Derivatives and Their Structural Assessment by NMR, X-Ray, and DFT Studies, *RSC Adv.*, 2023, **13**(10), 6747–6759, DOI: 10.1039/d3ra00137g.

63 S. Cheng, L. Wei, X. Zhao and J. Julson, Application, Deactivation, and Regeneration of Heterogeneous Catalysts in Bio-Oil Upgrading, *Catalysts*, 2016, **6**(12), 195, DOI: 10.3390/catal6120195.

64 N. Khan, M. U. Khan, M. Shadab, M. B. Siddiqui and Z. N. Siddiqui, CCDC 2416550: Polyaniline-functionalized biochar (PANI@ALB) as heterogeneous acid–base bifunctional catalyst for one-pot cascade reactions under green reaction conditions, 2025, DOI: 10.1039/d5su00279f.